Anal Bioanal Chem (2017) 409:1093–1100
DOI 10.1007/s00216-016-0028-5

RESEARCH PAPER

A plasmonic ELISA for the naked-eye detection of chromium ions in water samples

Cuize Yao[1,2] · Shiting Yu[1] · Xiuqing Li[1] · Ze Wu[1] · Jiajie Liang[1] · Qiangqiang Fu[1] · Wei Xiao[1] · Tianjiu Jiang[3] · Yong Tang[1]

Received: 26 June 2016 / Revised: 22 September 2016 / Accepted: 11 October 2016 / Published online: 22 November 2016

Abstract Here, we describe the development of a triangular silver nanoprism (AgNPR) etching-based plasmonic ELISA for the colorimetric determination of Cr(III) levels in environmental water samples. This involved the creation of a novel signal generation system (substrate reaction solution) for a competitive ELISA in which hydrogen peroxide (H_2O_2) is used to etch triangular AgNPRs, inducing a change in color. This is achieved by controlling the H_2O_2 concentration that remains after degradation by catalase, which is conjugated to the secondary antibody of the ELISA. Because the degree of color change and the shift in the absorption spectrum of the substrate reaction solution are closely correlated with the Cr(III) concentration, this plasmonic ELISA can be used not only for the quantification of Cr(III) concentrations ranging from 3.13 to 50 ng/mL, with a limit of detection (LOD) of 3.13 ng/mL, but also for the visual detection (indicated by a color change from blue to mauve) of Cr(III) with a sensitivity of 6.25 ng/mL by the naked eye. Therefore, the plasmonic ELISA developed in this work represents a new strategy for heavy metal ion detection and has high potential applicability in resource-constrained areas.

Keywords Triangular silver nanoprism · Colorimetric · Plasmonic ELISA · Chromium ion

Cuize Yao and Shiting Yu contributed equally to this work.

Electronic supplementary material The online version of this article (doi:10.1007/s00216-016-0028-5) contains supplementary material, which is available to authorized users.

✉ Tianjiu Jiang
tjiangtj@jnu.edu.cn

✉ Yong Tang
tyjaq7926@163.com

[1] Department of Bioengineering, Guangdong Province Key Laboratory of Molecular Immunology and Antibody Engineering, Jinan University, Guangzhou, Guangdong 510632, China

[2] Medical Genetic Centre, Guangdong Women and Children Hospital, Guangzhou, Guangdong 510010, China

[3] Key Laboratory of Aquatic Eutrophication and Control of Harmful Algal Blooms of Guangdong Higher Education Institute, Jinan University, Guangzhou, Guangdong 510632, China

Introduction

Due to rapid industrial development, more and more nondegradable heavy metal ions (e.g., Cr^{3+}, Pb^{2+}, Hg^{2+}, Cu^{2+}, Ni^{2+}, and Cd^{2+}) are being discharged into water and soil by various routes [1], where they remain indefinitely, exposing ecological systems and food chains to high levels of pollution [2–4]. Chromium (Cr) is a regulated toxic heavy metal that exists mainly in two oxidation states, Cr(III) and Cr(VI). Although Cr(III) is less toxic than Cr(VI), it can accumulate to high levels in the environment, and high concentrations of Cr(III) can bind to DNA, which has a detrimental effect on cellular structures and damages cellular components [5, 6]. Moreover, Cr(III) can be oxidized to the more toxic Cr(VI), which has been linked to disease states including neurological damage, birth defects, lung cancer, liver cancer, and esophageal cancer, and can thus increase the regional incidence of cancer and infant deformities [7–9]. Because Cr(VI) cannot be chelated with ethylenediaminetetraacetic acid (EDTA) and easily reduced to Cr(III) through pretreatment, a monoclonal antibody was designed to target Cr(III)–EDTA [4, 10]. Therefore, the development of an easy readout method to detect Cr(III) could be significant for human health.

Various analytical methods have been reported to detect heavy metal ions, including inductively coupled plasma mass

spectrometry (ICP-MS) [11, 12], flow injection analysis [13], atomic absorption, atomic emission, and flame emission spectrometry [14, 15], fluorescence spectrometry [16], DNAzyme biosensors [17, 18], aptamer biosensors [19], enzyme-linked immunosorbent assays (ELISAs) [20, 21], and immunochromatographic biosensors [22–24]. Although these analytical methods have high sensitivity and specificity, most require well-trained operators and expensive instruments. Therefore, a more cost-effective and user-friendly analytical method with a straightforward readout would be widely applicable and highly desirable in the study of heavy metal ions.

Metal nanoparticles, such as gold nanoparticles (AuNPs) and silver nanoparticles (AgNPs), are commonly used in plasmonic nanosensors, as they exhibit excellent localized surface plasmon resonance (LSPR). LSPR is an optical property of nanomaterials that is strongly dependent upon the morphology and aggregation state of the nanostructures. The LSPR state of plasmonic nanoparticles can indicate the presence or absence of target biomolecules. Furthermore, changes in the LSPR state of plasmonic nanoparticles are linearly correlated with the concentrations of analytes [25–27]. Recent advances in plasmonic nanosensors have it possible to develop a series of rapid on-site detection assays with useful properties [28–31] such as a visible readout and high sensitivity and specificity [32–34]. Among these plasmonic nanosensors, triangular silver nanoprism (AgNPR) etching-based plasmonic nanosensors are of particular interest because their lateral dimensions greatly exceed their thickness, favoring highly tunable LSPR [35, 36]. Xia et al. described a glucose plasmonic nanosensor in which H_2O_2 produced by a glucose oxidase system acts as an oxidant to etch the triangular AgNPRs into nanodiscs [34]. Glucose concentrations correlated well with the color change and the blueshift of the LSPR peak of the triangular AgNPRs [37]. Based on this method of generating H_2O_2 from the enzymatic oxidation of a glucose system, Liang et al. developed a highly sensitive triangular AgNPR etching-based plasmonic sandwich ELISA for the detection of prostate-specific antigen (PSA) [36].

Here, we introduce a triangular AgNPR-based plasmonic competitive ELISA to detect Cr(III) in water samples. This assay can be used for both the quantification and the visual assessment of Cr(III) levels by the naked eye. The plasmonic competitive ELISA we developed is a heavy metal ion sensing platform with two important advantages over other analytical methods. First, since the signals are positively and closely correlated with analyte concentrations, the readout can easily be evaluated and quantified. This represents a significant improvement in the user-friendliness of competitive immunoassays. In addition, the obvious blue-to-mauve changes can easily be distinguished by the naked eye, making this method cost-effective and suitable for heavy metal ion detection, even in resource-constrained areas.

Materials and methods

Materials and apparatus

Silver nitrate ($AgNO_3$, 99.8 %) was purchased from Sinoreagent (Shanghai, China). Trisodium citrate was obtained from Damaoreagent (Tianjin, China). Hydrogen peroxide (H_2O_2, 30 wt%), Tween-20, and $NaBH_4$ were purchased from GZ Chemical Reagent (Guangzhou, China). Catalase and polyvinylpyrrolidone (PVP, MW 40,000) were obtained from Sigma (St. Louis, MO, USA), respectively. Biotin-conjugated goat anti-mouse IgG (Ab_2) was purchased from Proteintech (Chicago, IL, USA). Dimethyl sulfoxide (DMSO) and 24-unit ethylene glycol functionalized with succinimidyl and maleimido ends (SM(PEG)24) were obtained from Thermo Scientific (Waltham, MA, USA). Catalase-Ab2 was prepared in our lab (the process is explained in the "Electronic supplementary material," ESM1). Chromium chloride (99.99 %) was obtained from Sigma–Aldrich (Milwaukee, WI, USA), and all other metal ions were purchased from Merck KGaA (Darmstadt, Germany). Anti-Cr(III)-iEDTA antibodies (Ab_1), Cr(III)-iEDTA-OVA, phosphate buffer (PBS, pH 7.4), and bicarbonate buffer (pH 9.6) were prepared in our laboratory [4]. Isothiocyanobenzyl-EDTA (iEDTA) was purchased from Dojindo Laboratories (Kumamoto, Japan). Deionized water (Milli-Q grade, Millipore, Billerica, MA, USA) with a resistivity of 18.2 MΩ cm was used throughout this study. For the ELISA, 96-well polystyrene plates were purchased from Guangzhou Jet Bio-Filtration Co., Ltd. (Guangzhou, China). The triangular AgNPRs were characterized by transmission electron microscopy (TEM) using a Philips (Eindhoven, Netherlands) TECNAI-10 transmission electron microscope operating at an acceleration voltage of 120 kV. The LSPR spectra of the resulting solutions in 96-well plates were collected by a Synergy H1 hybrid multimode microplate reader (Bio-Tek Instruments, Inc., Winooski, VT, USA). Inductively coupled plasma mass spectrometry (ICP-MS, Thermo Fisher Scientific, Waltham, MA, USA) was used to confirm sample composition.

Preparation of substrate reaction solutions (solution A and solution B)

Solution A refers to 20 μM H_2O_2 and solution B to the triangular AgNPRs. Triangular AgNPRs were prepared as previously described [36, 37]. Briefly, 50 μL $AgNO_3$ (0.1 M), 750 μL sodium citrate (0.1 M), and 120 μL H_2O_2 (30 wt%) were added one at a time to a conical flask containing 49.08 mL of deionized water. The solution was vigorously stirred on a magnetic stir plate at room temperature. After the rapid addition of 400 μL $NaBH_4$ (100 mM), the solution changed gradually from colorless to light yellow and, after approximately 20 min, to blue, indicating the formation of triangular AgNPRs. The resultant triangular AgNPRs were stored at 4 °C until use.

Competitive Cr(III) assay

To detect Cr(III) via plasmonic ELISA, 96-well microplates were pre-coated with the antigen Cr(III)-iEDTA-OVA diluted in bicarbonate buffer (100 mM, pH 9.6) overnight at 4 °C. After washing the microplates three times with wash buffer (0.1 % Tween-20 in PBS) to remove unbound Cr(III)-iEDTA-OVA, the plates were blocked with blocking buffer (1 % BSA in PBS) at 37 °C for 1 h, followed by three additional washes. Next, 50 μL of different concentrations of Cr(III) diluted in 5 μM EDTA-Na_2 (prepared in our lab) were added to the microplates, followed by 50 μL anti-Cr(III)-iEDTA monoclonal antibodies (Ab_1, prepared in our lab). Microplates were incubated at 37 °C for 1 h and then washed three times to remove unbound Ab_1. Next, 200 μL catalase-Ab_2 were added to each well, which were then incubated at 37 °C for 1 h. Following incubation, the microplates were washed, and 100 μL substrate solution A were added to each well. Fifty microliters of substrate solution B were added after 30 min and allowed to mix with solution A in the plate at room temperature for 15 min before the resulting LSPR spectrum was imaged and analyzed.

Analysis of spiked samples

Water samples for the experiment were obtained from the Pearl River (Guangzhou, China) or were tap water (Tianhe, China). Serially diluted Cr(III) was spiked into the tap water and Pearl River water samples with 5 μM EDTA-Na_2, and the samples were analyzed using the plasmonic ELISA. These Cr(III)-spiked water samples were also assessed by ICP-MS.

Colorimetric differentiation of Cr(III) from other metal ions

To evaluate the specificity of the triangular AgNPR-based plasmonic nanoimmunosensor, a series of metal ions, including Zn^{2+}, Co^{2+}, Al^{3+}, Mg^{2+}, Ca^{2+}, Pb^{2+}, and Fe^{2+}, were tested at concentrations of 10 ng/mL.

Results and discussion

Scheme of the plasmonic ELISA

The basic principle of the plasmonic ELISA Cr(III) detection system is illustrated in Fig. 1. In the absence of Cr(III)-EDTA

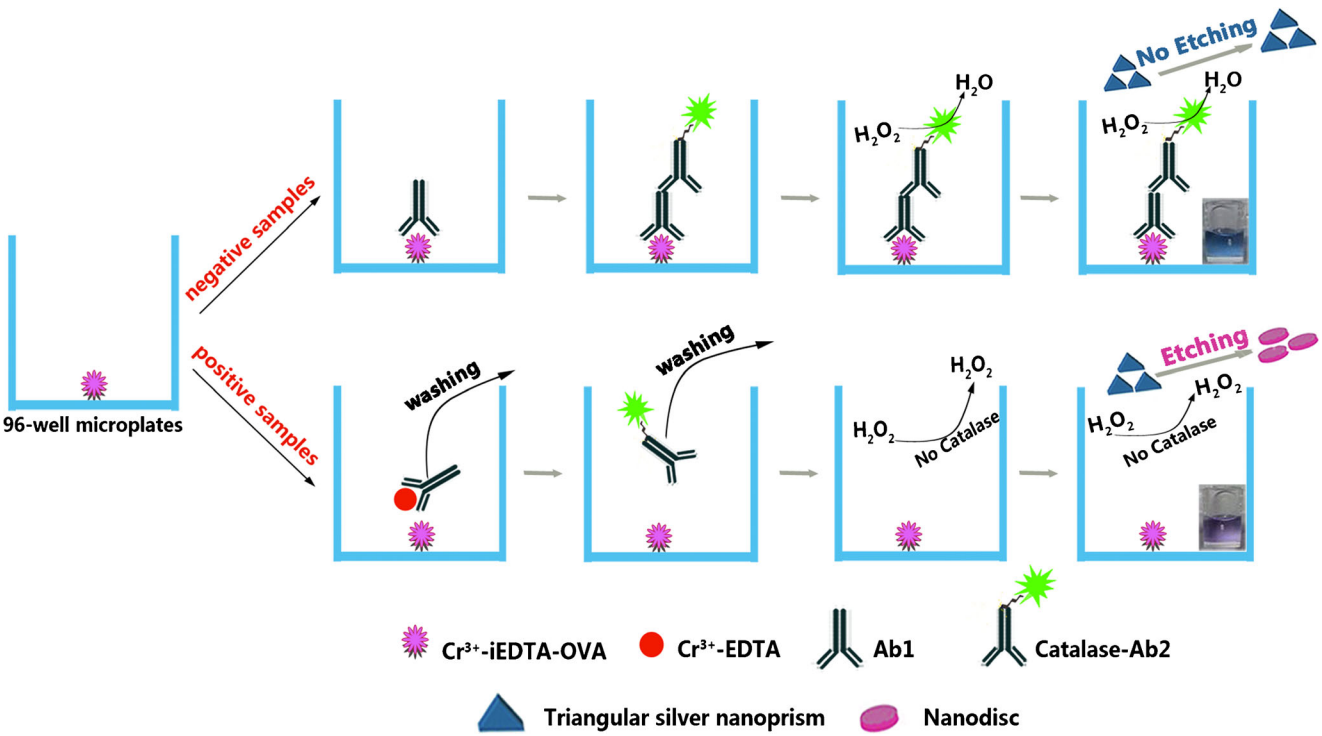

Fig. 1 Schematic of the plasmonic Cr(III) ELISA. For negative samples (no Cr(III)-EDTA), the catalase-Ab_2 bound on the microplate through immunoreactions degrades the H_2O_2 in solution A. As a result, H_2O_2 in solution A is consumed, no AgNPR etching occurs, and no color change or spectral shift is detected. For positive samples (containing Cr(III)-EDTA), analytes and antigens coating the microplate competitively bind Ab_1, leading to a decrease in catalase-Ab_2 captured on the microplates. H_2O_2 in solution A is not completely consumed; it maintains a relatively high, Cr(III)-dependent concentration, etching triangular AgNPRs of solution B. Subsequently, the reaction solution changed color from blue to mauve, and its LSPR peak gradually blueshifted

(negative samples), the anti-Cr(III)-iEDTA antibodies (Ab_1) are captured by the coating antigens (Cr(III)-iEDTA-OVA) and bind the added catalase conjugated to Ab_2 (catalase-Ab_2). When substrate solutions A and B are then successively added to the microplate, the H_2O_2 in solution A is degraded by the bound catalase so that the nanoparticles in solution B maintain their triangular shape and the color remains blue.

When samples containing Cr(III)-EDTA are added to the precoated microplates (positive samples), the Cr(III)-EDTA in the samples and the coating antigens competitively bind Ab_1. The free Cr(III)-EDTA-Ab_1 complexes are removed during the washes, resulting in a reduction in the amount of captured Ab_1 and thus less catalase-Ab_2 that is bound by the microplates. Therefore, the H_2O_2 from solution A remains at a higher level and can catalyze the etching of the triangular AgNPRs in solution B into nanodiscs, leading to a distinct color change (from blue to mauve) and an LSPR wavelength blueshift. Importantly, the extent of the color change was found to be correlated with the concentration of Cr(III) in the samples. The plasmonic ELISA can thus be used not only for Cr(III) quantification but also for the visual detection of Cr(III) by the naked eye.

H_2O_2-mediated etching of triangular AgNPRs

According to previous research [37], H_2O_2 can easily etch triangular AgNPRs because of its powerful oxidizing properties. To investigate the influence of the H_2O_2 concentration on the etching of triangular AgNPRs, the triangular AgNPRs were etched with different concentrations of H_2O_2 ranging from 0 to 100 μM (experimental details are explained in the ESM). As shown in Fig. 2a, as the concentration of H_2O_2 increases from 0 to 100 μM, the color of the reaction solution gradually changes from brilliant blue to mauve, and this

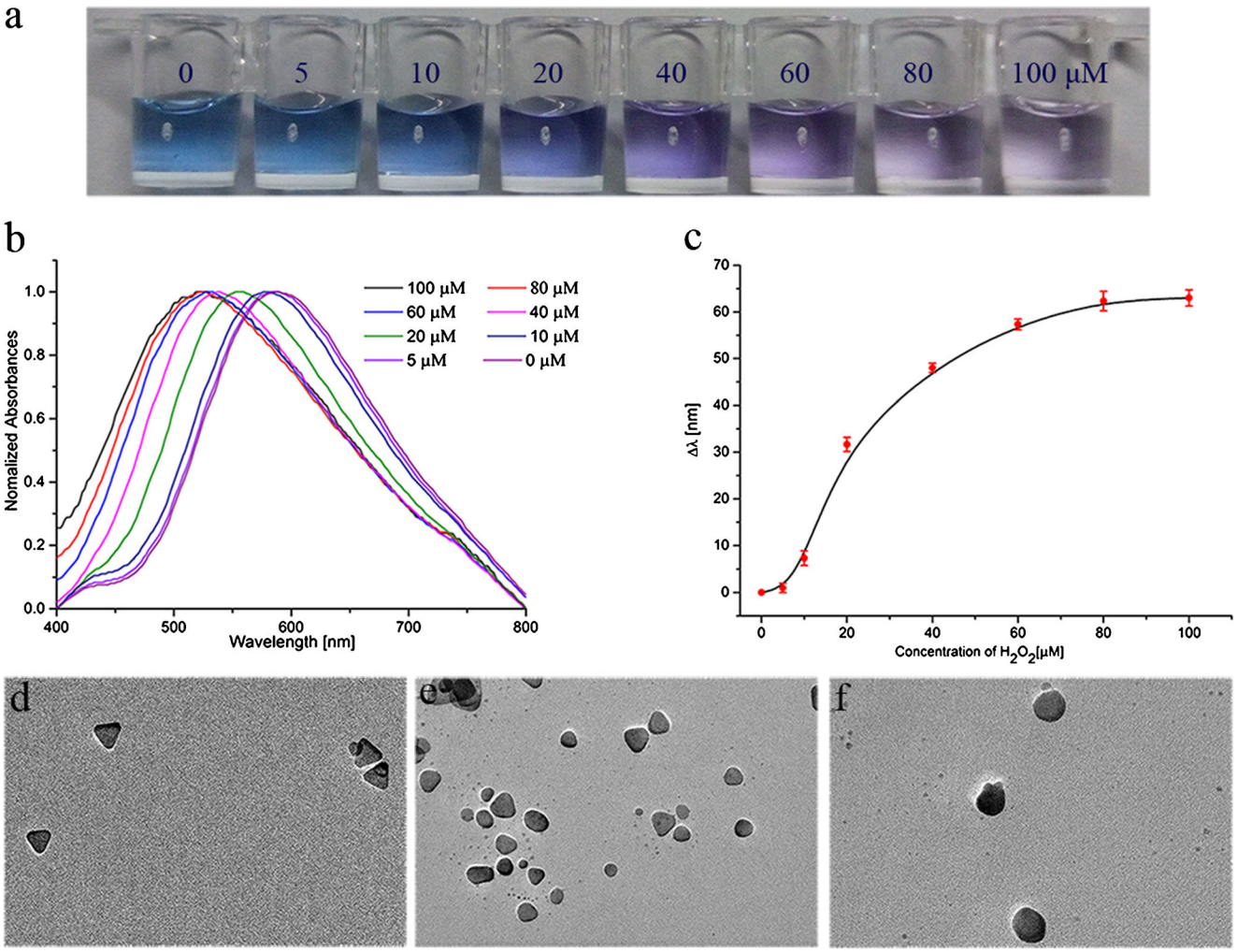

Fig. 2a–f Characterization of H_2O_2-mediated etching of triangular AgNPRs. **a** Color changes induced by triangular AgNPRs etched by different concentrations of H_2O_2 (0–100 μM). **b** Corresponding LSPR peaks of the triangular AgNPRs etched by different concentrations of H_2O_2. **c** Standard curve plotting the relationship between the LSPR peak blueshift of the triangular AgNPRs and the concentration of H_2O_2. **d–f** TEM images of triangular AgNPRs etched by 0 μM (**d**), 50 μM (**e**), or 100 μM (**f**) of H_2O_2, respectively. Scale bar is 50 nm. The triangular AgNPRs become increasingly round as the H_2O_2 concentration increases

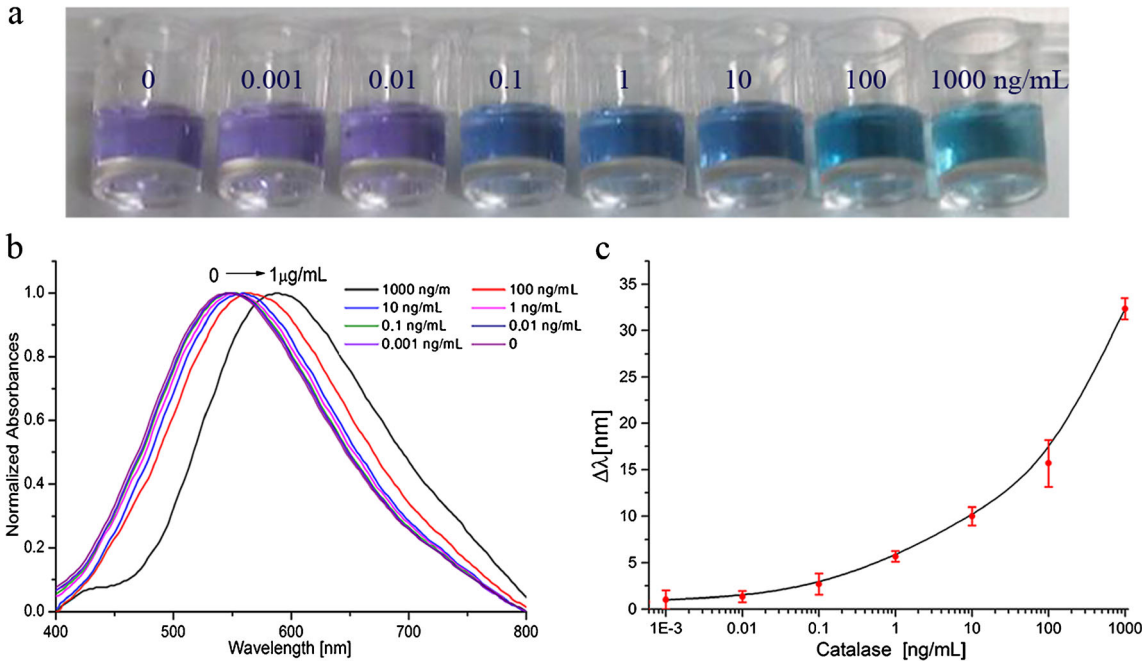

Fig. 3a–c H_2O_2 etching of triangular AgNPRs in the presence of different catalase concentrations. **a** Color change induced by H_2O_2-etched triangular AgNPRs exposed to a serially diluted catalase. As the catalase concentration increased, H_2O_2 levels decreased, and the color of the resulting solution changed from mauve to blue. **b** Corresponding LSPR peaks of triangular AgNPRs. As the catalase concentration increased (0–1,000 ng/mL), the LSPR absorbance of the triangular AgNPRs was redshifted. **c** Relationship between the AgNPR LSPR peak shift and the catalase concentration

change can be clearly distinguished starting at 20 μM H_2O_2 by the naked eye. Additionally, the LSPR peak exhibits a gradual blueshift (Fig. 2b–c). The degree of LSPR blueshift and the color change were highly dependent on the concentration of H_2O_2. TEM images revealed that the morphology of the triangular AgNPRs gradually changed from triangular to round when they were etched with increasing concentrations of H_2O_2 (Fig. 2d–f).

Catalase-dependent triangular AgNPR etching

To determine the effects of the catalase concentration, the degree of H_2O_2-mediated etching of triangular AgNPRs and the associated LSPR peaks were evaluated in the presence of different catalase concentrations ranging from 0 to 1,000 ng/mL (experimental details are provided in the ESM). As shown in Fig. 3a, a distinct color change from mauve to blue was observed as the concentration of catalase increased, and the color change process was highly dependent on the catalase concentration. Moreover, the LSPR peaks of the triangular AgNPRs were redshifted, and higher catalase concentrations produced greater redshifts of the LSPR peak (Fig. 3b–c).

Cr(III) detection by competitive plasmonic ELISA

After demonstrating that H_2O_2 could etch triangular AgNPRs and cause a color change, we applied this competitive ELISA

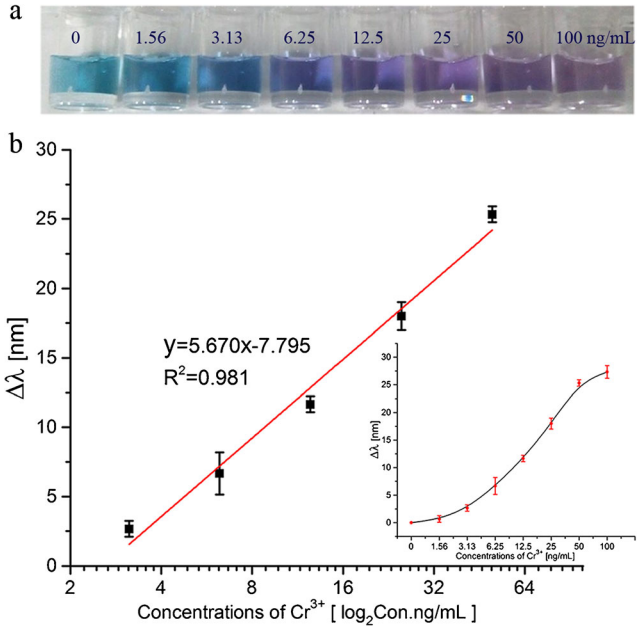

Fig. 4a–b Detection of different Cr(III) concentrations using the plasmonic nanoimmunosensor ELISA. **a** The etching of the triangular AgNPRs induced a color change from blue to mauve as the concentration of Cr(III) increased. **b** Calibration curve of the plasmonic nanoimmunosensor. The *inset* in **b** plots the relationship between the LSPR peak blueshift of the triangular AgNPRs and the concentration of Cr(III). Each value represents the mean of the values obtained in three replicates, and *error bars* indicate the standard deviation based on three independent measurements

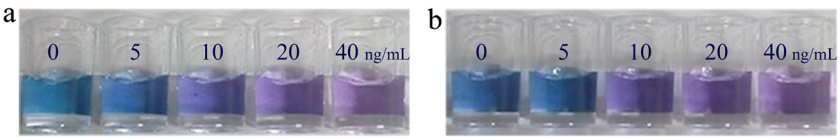

Fig. 5a–b Color change from blue to mauve in the detection of Cr(III) spiked into tap water (**a**) or Pearl River water (**b**)

Table 1 Detection of Cr(III) in tap water and Pearl River water samples

Samples	Actual Cr(III) concentration (ng/mL)	Cr(III) concentration detected by ICP-MS (ng/mL)	Recovery by ICP-MS (%)	Cr(III) concentration detected by plasmonic ELISA (ng/mL)	Recovery by plasmonic ELISA (%)	Coefficient of variation (%)
Spiked tap water	0	0	0	0.45		
	5	3	60	3.58 ± 0.19	71.6	5.3
	10	9	90	9.91 ± 0.61	99.1	6.2
	20	22	110	20.55 ± 1.11	102.7	5.4
	40	43	107.5	40.41 ± 2.78	101.0	6.9
Spiked Pearl River water	0	0	0	0.45		
	5	3	60	3.44 ± 0.25	68.8	7.2
	10	10	100	9.73 ± 0.67	97.3	6.9
	20	21	105	21.12 ± 1.57	105.6	7.4
	40	42	105	40.73 ± 3.04	101.8	7.5

to the detection of Cr(III). Different concentrations of Cr(III) ranging from 0 to 100 ng/mL were chelated with EDTA and analyzed using the plasmonic competitive ELISA. In this case, the color of the resulting solution was blue when Cr(III) concentration was low (0 ng/mL), and changed to mauve when the Cr(III) concentration reached 6.25 ng/mL (Fig. 4a). Concentrations as low as 6.25 ng/mL Cr(III) were detectable by the naked eye. The LSPR peak blueshift of the triangular AgNPRs increased as the concentration of Cr(III) increased in the range 3.13 ng/mL to 50 ng/mL, and the lower LOD was determined as 3.13 ng/mL (Fig. 4b).

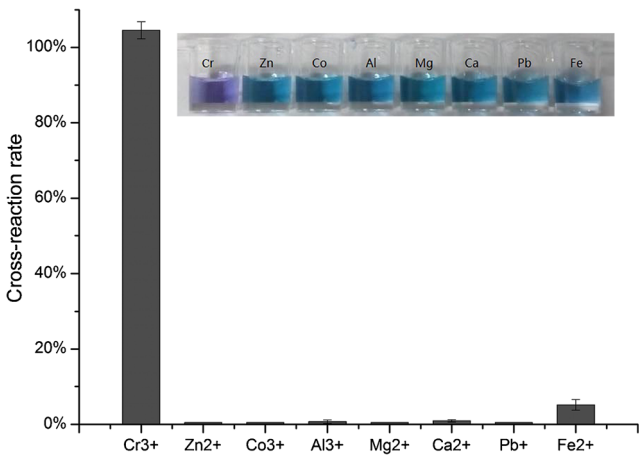

Fig. 6 Detection of other metal ions (Zn^{2+}, Fe^{2+}, Co^{2+}, Al^{3+}, Mg^{2+}, Ca^{2+}, Pb^{2+}, and Cu^{2+}) using the plasmonic Cr(III) ELISA to determine cross-reactivity. The cross-reactivity rate is expressed as (Cr(III)/100)×100 %. *Inset* shows the final reaction solution of samples containing 10 ng/mL of the tested metal ion

Cr(III) detection in spiked samples

The tap water and Pearl River samples were mixed with 5 μM EDTA and then spiked with 0, 5, 10, 20, and 40 ng/mL Cr(III), respectively. These water samples were then analyzed by the plasmonic ELISA. As shown in Fig. 5a–b, an obvious color change occurred when the Cr(III) concentration reached 10 ng/mL. According to the LSPR blueshift of the triangular AgNPR solution, the plasmonic ELISA has a relatively high recovery (Table 1).

Selectivity for Cr(III)

The cross-reactivity of the immunoassay was assessed by detecting other metal ions, including Zn^{2+}, Co^{2+}, Al^{3+}, Mg^{2+}, Ca^{2+}, Pb^{2+}, and Fe^{2+}, at concentrations of 10 ng/mL. No distinguishable change in the color of the triangular AgNPR solution was observed in the presence of those other metal ions compared with the blank control. By measuring the blueshift in the absorbance spectrum, cross-reactivities of 0.73 %, 0.93 %, and 5.18 % were observed with Al^{3+}, Ca^{2+}, and Fe^{2+}, respectively (Fig. 6). The cross-reactivity rate is expressed as (Cr(III)/100)×100 %. The cross-reactivity rates of the other metal ions with Cr(III) were less than 0.73 %. These results confirm the high specificity of the triangular AgNPR-based plasmonic ELISA for the detection of Cr(III).

Table 2 Comparison of various methods of Cr(III) detection

Method	Linear range (ng/mL)	Limit of detection (ng/mL)	Reference
Plasmonic ELISA	3.13–50	6.25 3.13	This work
High-performance liquid chromatography (HPLC)	400–1000		[38]
Resonance Rayleigh scattering sensor	5×10^{-5}–5×10^{-4}	5×10^{-5}	[39]
Fluorescence-quenching immunochromatographic sensor	6.25–800	1.56	[22]
Raman scattering-based lateral flow immunoassay	10^{-6}–10^{-2}		[23]
ELISA	0.8–50	0.081	[40]
Flame atomic absorption spectrometric detection	-	2.1	[41]
Colloidal gold nanoparticle probe-based immunochromatographic assay	5–80	-	[4]

Comparison with existing methods

Compared to other analytical chromium detection methods (Table 2), the presented method offers a range of detection and an LOD comparable to those of several other methods. In addition to the quantification of relevant levels of Cr(III), the plasmonic ELISA offers several other advantages, including that it does not require expensive equipment and that it makes it possible to detect Cr(III) by eye due to the obvious color change from blue to mauve. Furthermore, the strategy employed by this method provides users with another option for the detection of heavy metal ions in resource-constrained areas.

Conclusions

In summary, we have presented a competitive plasmonic ELISA that accurately quantifies Cr(III) levels based on the LSPR wavelength shift of a triangular AgNPR reaction solution and allows Cr(III) levels to be assessed by the naked eye based on the color change of the solution. The signal was found to be positively correlated with the analyte concentration and allowed easy interpretation of the results. Because of its user-friendliness and the ability to observe the signal with the naked eye, this plasmonic ELISA could be the best option for Cr(III) detection in resource-limited regions. In the near future, the strategy developed in this assay should be applied to improve the detection of Cr(VI) and total chromium ions in complex biological matrices.

Acknowledgments This work was supported by the National Key Research and Development Program of China (2016YFD0500600), the Technology Research Program of Guangzhou City (201508020100), the Technology Research Program of Guangdong Province (2013B010404027), and the Guangdong Innovative and Entrepreneurial Research Team Program (201301S0105240297). This manuscript was edited and proof-read by NPG Language Editing.

Compliance with ethical standards

Conflict of interest The authors declare that they have no conflict of interest.

References

1. Rubio C, González-Iglesias T, Revert C, Reguera JI, Gutiérrez AJ, Hardisson A. Lead dietary intake in a Spanish population (Canary Islands). J Agric Food Chem. 2005;53(16):6543–9.
2. Järup L. Hazards of heavy metal contamination. Br Med Bull. 2003;68(1):167–82.
3. Li YT, Becquer T, Dai J, Quantin C, Benedetti MF. Ion activity and distribution of heavy metals in acid mine drainage polluted subtropical soils. Environ Pollut. 2009;157(4):1249–57.
4. Liu X, Xiang JJ, Tang Y, Zhang XL, Fu QQ, Zou JH, et al. Colloidal gold nanoparticle probe-based immunochromatographic assay for the rapid detection of chromium ions in water and serum samples. Anal Chim Acta. 2012;745:99–105.
5. Bere T, Chia MA, Tundisi JG. Effects of Cr III and Pb on the bioaccumulation and toxicity of Cd in tropical periphyton communities: implications of pulsed metal exposures. Environ Pollut. 2012;163:184–91.
6. Shi J, Chen H, Arocena JM, Whitcombe T, Thring RW, Memiaghe JN. Elemental sulfur amendment decreases bio-available Cr-VI in soils impacted by leather tanneries. Environ Pollut. 2016;212:57–64.
7. Kimbrough DE, Cohen Y, Winer AM, Creelman L, Mabuni C. A critical assessment of chromium in the environment. Crit Rev Environ Sci Technol. 1999;29(1):1–46.
8. Kocaoba S, Akcin G. Removal and recovery of chromium and chromium speciation with MINTEQA2. Talanta. 2002;57(1):23–30.
9. Farag AM, May T, Marty GD, Easton M, Harper DD, Little EE, et al. The effect of chronic chromium exposure on the health of Chinook salmon (*Oncorhynchus tshawytscha*). Aquat Toxicol. 2006;76(3):246–57.

10. WHO. The World Health Organization Quality of Life assessment (WHOQOL): position paper from the World Health Organization. Soc Sci Med. 1995;41(10):1403–9.
11. Burlingame AL, Boyd RK, Gaskell SJ. Mass spectrometry. Anal Chem. 1996;68(12):599–652.
12. Li YR, Pradhan NK, Foley R, Low GKC. Selective determination of airborne hexavalent chromium using inductively coupled plasma mass spectrometry. Talanta. 2002;57(6):1143–53.
13. Pressman MAS, Aldstadt JH. A comparative study of diffusion samplers for the determination of hexavalent chromium by sequential injection spectrophotometry. Microchem J. 2003;74(1):47–57.
14. Jackson KW, Mahmood TM. Atomic absorption, atomic emission, and flame emission spectrometry. Anal Chem. 1994;66(12):252R–79R.
15. Zhu XS, Hu B, Jiang ZC, Li MF. Cloud point extraction for speciation of chromium in water samples by electrothermal atomic absorption spectrometry. Water Res. 2005;39(4):589–95.
16. Yuan D-h, Guo X-j, Wen L, He L-s, Wang J-g, Li J-q. Detection of copper (II) and cadmium (II) binding to dissolved organic matter from macrophyte decomposition by fluorescence excitation-emission matrix spectra combined with parallel factor analysis. Environ Pollut. 2015;204:152–60.
17. Liu JW, Lu Y. A colorimetric lead biosensor using DNAzyme-directed assembly of gold nanoparticles. J Am Chem Soc. 2003;125(22):6642–3.
18. Wang ZD, Lee JH, Lu Y. Label-free colorimetric detection of lead ions with a nanomolar detection limit and tunable dynamic range by using gold nanoparticles and DNAzyme. Adv Mater. 2008;20(17):3263–7.
19. Wu YG, Zhan SS, Wang LM, Zhou P. Selection of a DNA aptamer for cadmium detection based on cationic polymer mediated aggregation of gold nanoparticles. Analyst. 2014;139(6):1550–61.
20. Xiang JJ, Zhai YF, Tang Y, Wang H, Liu B, Guo CW. A competitive indirect enzyme-linked immunoassay for lead ion measurement using mAbs against the lead–DTPA complex. Environ Pollut. 2010;158(5):1376–80.
21. Zhou Y, Tian XL, Li YG, Pan FG, Zhang YY, Zhang JH, et al. An enhanced ELISA based on modified colloidal gold nanoparticles for the detection of Pb (II). Biosens Bioelectron. 2011;26(8):3700–4.
22. Fu QQ, Tang Y, Shi CY, Zhang XL, Xiang JJ, Liu X. A novel fluorescence-quenching immunochromatographic sensor for detection of the heavy metal chromium. Biosens Bioelectron. 2013;49:399–402.
23. Liang JJ, Liu HW, Lan CF, Fu QQ, Huang CH, Luo Z, et al. Silver nanoparticle enhanced Raman scattering-based lateral flow immunoassays for ultra-sensitive detection of the heavy metal chromium. Nanotechnology. 2014;25(49):495501.
24. Tang Y, Zhai Y-F, Xiang J-J, Wang H, Liu B, Guo C-W. Colloidal gold probe-based immunochromatographic assay for the rapid detection of lead ions in water samples. Environ Pollut. 2010;158(6):2074–7.
25. Tokel O, Inci F, Demirci U. Advances in plasmonic technologies for point of care applications. Chem Rev. 2014;114(11):5728–52.
26. Wang J, Lu J, Su S, Gao J, Huang Q, Wang L, et al. Binding-induced collapse of DNA nano-assembly for naked-eye detection of ATP with plasmonic gold nanoparticles. Biosens Bioelectron. 2015;65:171–5.
27. Wei L, Wang X, Li C, Li X, Yin Y, Li G. Colorimetric assay for protein detection based on "nano-pumpkin" induced aggregation of peptide-decorated gold nanoparticles. Biosens Bioelectron. 2015;71:348–52.
28. Zhao L, Jin Y, Yan ZW, Liu YY, Zhu HJ. Novel, highly selective detection of Cr(III) in aqueous solution based on a gold nanoparticles colorimetric assay and its application for determining Cr(VI). Anal Chim Acta. 2012;731:75–81.
29. Ye YJ, Liu HL, Yang LB, Liu JH. Sensitive and selective SERS probe for trivalent chromium detection using citrate attached gold nanoparticles. Nanoscale. 2012;4(20):6442–8.
30. Chen GH, Chen WY, Yen YC, Wang CW, Chang HT, Chen CF. Detection of mercury (II) ions using colorimetric gold nanoparticles on paper-based analytical devices. Anal Chem. 2014;86(14):6843–9.
31. Cecchin D, de La Rica R, Bain RES, Finnis MW, Stevens MM, Battaglia G. Plasmonic ELISA for the detection of gp120 at ultra-low concentrations with the naked eye. Nanoscale. 2014;6(16):9559–62.
32. Elghanian R, Storhoff JJ, Mucic RC, Letsinger RL, Mirkin CA. Selective colorimetric detection of polynucleotides based on the distance-dependent optical properties of gold nanoparticles. Science. 1997;277(5329):1078–81.
33. De La Rica R, Stevens MM. Plasmonic ELISA for the ultrasensitive detection of disease biomarkers with the naked eye. Nat Nanotechnol. 2012;7(12):821–4.
34. Fu Q, Wu Z, Xu F, Li X, Yao C, Xu M, et al. A portable smart phone-based plasmonic nanosensor readout platform that measures transmitted light intensities of nanosubstrates using an ambient light sensor. Lab Chip. 2016;16(10):1927–33.
35. Zhang Q, Li N, Goebl J, Lu ZD, Yin YD. A systematic study of the synthesis of silver nanoplates: is citrate a "magic" reagent? J Am Chem Soc. 2011;133(46):18931–9.
36. Liang JJ, Yao CZ, Li XQ, Wu Z, Huang CH, Fu QQ, et al. Silver nanoprism etching-based plasmonic ELISA for the high sensitive detection of prostate-specific antigen. Biosens Bioelectron. 2015;69:128–34.
37. Xia YS, Ye JJ, Tan KH, Wang JJ, Yang G. Colorimetric visualization of glucose at the submicromole level in serum by a homogenous silver nanoprism–glucose oxidase system. Anal Chem. 2013;85(13):6241–7.
38. Ali I, Aboul-Enein HY. Speciation of arsenic and chromium metal ions by reversed phase high performance liquid chromatography. Chemosphere. 2002;48(3):275–8.
39. Chen M, Cai HH, Yang F, Lin D, Yang PH, Cai J. Highly sensitive detection of chromium (III) ions by resonance Rayleigh scattering enhanced by gold nanoparticles. Spectrochim Acta A. 2013;118C(2):776–81.
40. Yu S, Xiao W, Fu Q, Wu Z, Yao C, Shen H, et al. A portable chromium ion detection system based on a smartphone readout device. Anal Methods. 2016.
41. Leśniewska B, Trzonkowska L, Zambrzycka E, Godlewska-Żyłkiewicz B. Multi-commutation flow system with on-line solid phase extraction exploiting the ion-imprinted polymer and FAAS detection for chromium speciation analysis in sewage samples. Anal Methods. 2014;7(4):1517–26.